Journal of
Materials Chemistry C

PAPER

View Article Online
View Journal | View Issue

Check for updates

Cite this: *J. Mater. Chem. C*, 2017, 5, 10061

Discrete face-to-face stacking of anthracene inducing high-efficiency excimer fluorescence in solids *via* a thermally activated phase transition†

Yue Shen,[a] Haichao Liu,[a] Shitong Zhang,[a] Yu Gao,[a] Bao Li,[a] Yan Yan,[b] Yongsheng Hu,[c] Lijuan Zhao[a] and Bing Yang *[a]

It is always a challenge for planar polycyclic aromatic molecules to achieve high efficiency in solids owing to their frequent encounter with aggregation-caused quenching (ACQ). An anthracene derivative with one-side *meta*-substituted triphenylamine (TPA) was found to show high-efficiency excimer fluorescence (η_{PL} = 76.8%) in G-phase (green) crystals as well as a long lifetime, in sharp contrast with that of a monomer in a doped film (η_{PL} = 36.6%) and that of B-phase (blue) crystals (η_{PL} = 8.1%). In essence, the excimer-induced enhanced emission can be ascribed to the special intermolecular stacking in the solid state, namely, discrete antiparallel dimeric stacks between anthracene moieties in G-phase crystals, which are responsible for greatly suppressed non-radiative deactivation due to a uniform emissive state preventing the formation of an energy-trapping "dark" state. Moreover, a G-phase could be obtained through a thermally-activated phase transition from B-phase crystals, corresponding to the completely synchronized change of fluorescence properties. The present results consolidate a novel strategy of designing discrete dimeric stacking of planar polycyclic aromatic molecules to achieve high-efficiency fluorescence in the solid state by an excimer-induced enhanced emission (EIEE) mechanism.

Received 19th July 2017,
Accepted 30th August 2017

DOI: 10.1039/c7tc03229c

rsc.li/materials-c

Introduction

π-Conjugated organic aromatic molecules and polymers are generally used as light-emitting materials for many applications in organic light-emitting diodes (OLEDs), organic field-effect light-emitting transistors (OFLTs), organic lasers, biological imaging, chemo- and bio-sensors, and so on.[1–8] In most cases, these planar polycyclic aromatic compounds are apt to encounter aggregation-caused quenching (ACQ) in the solid-state due to the strong intermolecular π–π stacking interactions, resulting in the excited-state energy decay of the aggregates *via* non-radiative channels.[9–11] To be more exact, intermolecular π–π stacking prompts the formation of such low- or non-emissive species as an excimer, which is the low-lying energy-trapping "dark" state responsible for the most common fluorescence quenching in solid states.[12,13] Traditionally, the excimer formation is usually prevented as best as possible in organic polycyclic aromatic light-emitting materials by chemical or physical approaches. For instance, bulky-substitution, host–guest doping and molecular encapsulation are usually employed to suppress intermolecular π–π stacking between fluorophores for the efficient emission from monomer species.[14–19]

Although excimer formation quenches fluorescence from the traditional viewpoint, a few cases of high-efficiency excimer fluorescence have been reported recently. For example, our

---

[a] *State Key Laboratory of Supramolecular Structure and Materials, College of Chemistry, Jilin University, Changchun, 130012, P. R. China. E-mail: yangbing@jlu.edu.cn; Fax: +86-431-85168502; Tel: +86-431-85193421*
[b] *State Key Laboratory of Inorganic Synthesis and Preparative Chemistry, College of Chemistry, Jilin University, Changchun, 130012, P. R. China*
[c] *State Key Laboratory of Luminescence and Applications, Changchun Institute of Optics, Fine Mechanics, and Physics, Chinese Academy of Sciences, Changchun, 130033, P. R. China*

† Electronic supplementary information (ESI) available: The details of the synthesis of mTPA-9-AN; absorption spectra of TPA and AN; PL spectra and lifetimes of mTPA-9-AN in different proportions of water; lifetimes of mTPA-9-AN in different solutions; the PL spectrum and lifetimes of mTPA-9-AN of 1 wt% in PMMA; the excitation spectra of B- and G-phase crystals; crystallographic data and structure refinements of B- and G-phase crystals; stacked structure of B- and G-phase crystals; The k_r and k_{nr} of the doped film, B- and G-phase crystals; lifetimes of B-phase crystals at different temperatures; the PL spectrum and lifetime of heat-treated B-phase crystals at room temperature; ^{1}H NMR spectra of B-phase crystals before and after annealing, melted B-phase and G-phase crystals, G-phase crystals after different irradiation times; ground state geometries of monomers and frontier orbitals; NTOs of monomers; configuration of B- and G-phase dimers; schematic diagram of potential energy surfaces of B- and G-phase dimers; geometries of the ground state and the excited state of the G-phase dimer; the labels of atoms in B- and G-phase dimers; excitation, PL and transient PL spectra of TPA-AN. CCDC 1551980 and 1551981. For ESI and crystallographic data in CIF or other electronic format see DOI: 10.1039/c7tc03229c

group has reported an anthracene derivative, 2-(anthracen-9-yl)thianthrene (2-TA-AN), which demonstrates spatially-isolated antiparallel pairwise stacks of anthracene in crystals.[20] This crystal shows very highly efficient excimer fluorescence with a photoluminescence quantum yield (η_{PL}) of 80%. Recently, the Yoshizawa group designed a V-shaped anthracene derivative with three butyl groups, also exhibiting anthracene-excimer characteristic emission with a η_{PL} as high as 72% in the solid state.[21] A common feature in these molecules is that discrete dimeric stacks of anthracene exist in the crystal structure, which may contribute to the high-efficiency excimer fluorescence. As a whole, studies about excimer systems especially for high-efficiency fluorescence are still fairly rare, and a lot of experimental and theoretical efforts should be made toward a better understanding of excimer formation, structure–property relationships, future applications, *etc.*[22–26]

As we know, 4-(anthracen-9-yl)-*N*,*N*-diphenylaniline (TPA-AN) has been applied in OLEDs as an organic light-emitting layer, and its solids (powder and crystal) exhibit blue emission without excimer formation (Fig. S22, ESI†).[27,28] To form an anthracene excimer in the solid state, our strategy of molecular design is that the candidate should be composed of two moieties: planar aromatics (π-moiety) and a one-side substituent moiety. On the one hand, the π-moiety with only one-sided substitution is appropriate for dimer formation with antiparallel superposition of π–π stacking as large and close as possible; on the other hand, the one-sided substituent can serve as a spacer to separate dimers from each other, guaranteeing discrete and uniform dimeric stacking of the π-moiety. Conceivably, the size and orientation of the side substituent should play a crucial role in the spatially isolated dimeric stack formation to realize enhanced excimer emission. Thereby, we changed the substituent position of the triphenylamine (TPA) groups from a *para*- to a *meta*-linkage (relative to diphenylaniline), obtaining another new anthracene derivative, 3-(anthracen-9-yl)-*N*,*N*-diphenylaniline (**mTPA-9-AN**), as shown in Fig. 1a. Fortunately, two types of crystal phases were obtained with blue and green fluorescence under UV irradiation, corresponding to blue (B-) and green (G-) phase crystals, respectively. Both of these crystals possessed dimeric anthracene-stacking structures according to single-crystal X-ray diffraction (XRD). The G-phase prefers the face-to-face configuration of the anthracene dimer while the B-phase exhibits an edge-to-face arrangement of dimeric anthracenes. As a result, the G-phase results in largely red-shifted, broadened and structureless excimer fluorescence relative to that of the B-phase. Importantly, it is inspiring that G-phase crystals also display high-efficiency excimer fluorescence with a η_{PL} of 76.8%, which is over nine times higher than the 8.1% of B-phase crystals.[29] What is more, G-phase crystals could be obtained from B-phase crystals by heating, which may provide a new pathway to realize excimer-induced enhanced emission (EIEE) through thermally-activated phase transition. This phase transition from B-phase to G-phase crystals was accompanied by an almost completely synchronized change in the fluorescence properties (spectrum, efficiency and lifetime), which sufficiently indicates that the discrete face-to-face dimeric stacking of anthracene is responsible for the high-efficiency excimer fluorescence. In particular, high-efficiency excimer emission from a thermally-activated phase transition will produce some intriguing applications, as a result of the unique excimer fluorescence characteristics. The experimental and theoretical details will be presented below.

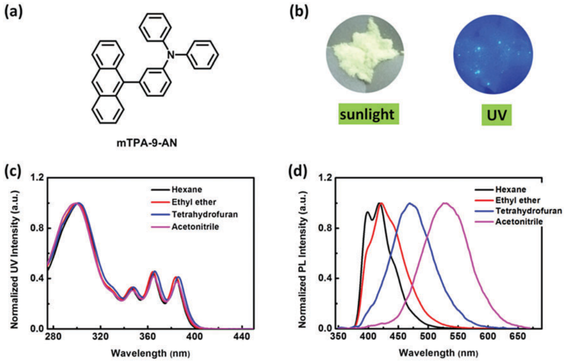

Fig. 1 (a) Molecular structure of **mTPA-9-AN**. (b) Photographs of **mTPA-9-AN** powder under sunlight (left) and 365 nm UV light (right). (c) Solvatochromic UV/Vis absorption spectra. (d) Solvatochromic PL spectra. The concentrations of the solutions were controlled to about 1×10^{-5} mol L^{-1}.

Results and discussion

Photophysical properties

The **mTPA-9-AN** compound was synthesized through a Suzuki coupling route as shown in the ESI.† The UV/Vis absorption spectra of **mTPA-9-AN** in different solvents were firstly examined, exhibiting two distinct absorption bands: one centered around 275–337 nm and the other around 337–400 nm (Fig. 1c). These two absorption bands correspond to those of the isolated TPA and anthracene (AN), respectively (Fig. S1, ESI†), indicating that the electron communication between TPA and AN is almost interrupted due to the *meta*-linkage mode in **mTPA-9-AN**. The photoluminescence (PL) spectra maxima demonstrate an obvious solvatochromic shift of over 112 nm from 418 nm in hexane to 530 nm in acetonitrile with the increase of solvent polarity, together with the gradual disappearance of vibrational fine structures, indicating a transformation of the excited state character from the locally-excited (LE) state in a low-polarity solvent to the charge-transfer (CT) state in a high-polarity one (Fig. 1d). Therefore, it can be inferred that the meta-linkage between TPA and AN effectively results in a typical CT character of the emissive state at medium-polarity.

Very interestingly, the **mTPA-9-AN** powder under UV irradiation (365 nm) showed two kinds of emission colors of blue and green (Fig. 1b), and they could be clearly distinguished by the naked eye. Based on this observation, we supposed that there were two types of possible aggregations in the solid-state powder. Further efforts were made to grow crystalline samples by the solvent evaporation process. We added the **mTPA-9-AN** powder into the compositional solvents of dichloromethane/methanol (2 : 1, v/v). About five days later, mixed crystals including B-phase and G-phase crystals were collected and manually separated according to their different

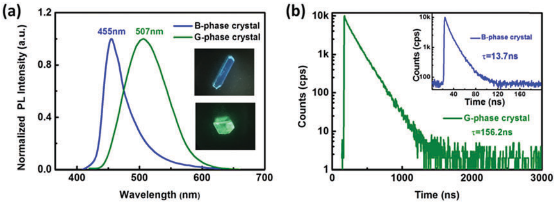

Fig. 2 The crystal spectra of the B-phase and G-phase. (a) PL spectra and photographs of B-phase (top) and G-phase (bottom) crystals under UV light (365 nm). (b) Transient PL spectra.

shapes and emissions under UV excitation (λ = 365 nm). One was a stripe-like crystal with blue fluorescence (λ_{max} = 455 nm), while the other was a cuboid-like crystal with green fluorescence (λ_{max} = 507 nm), as shown in Fig. 2a. Comparing the PL spectra of the crystals, the G-phase exhibited a markedly bathochromic shift (52 nm) relative to the B-phase. Moreover, time-resolved fluorescence (Fig. 2b) revealed a mono-exponential decay of G-phase crystals with only a single lifetime as long as τ = 156.2 ns, which was far longer than those of B-phase crystals (τ = 13.7 ns) and its tetrahydrofuran (THF) solution (τ = 12.4 ns) (Fig. S4, ESI†). Compared with the B-phase crystals, the largely red-shifted, broadened, and structureless PL spectral behaviors as well as long lifetimes of the G-phase crystals are in good accordance with the characteristics of a "sandwich" anthracene excimer.[19,30,31] More importantly, the G-phase crystals displayed high-efficiency excimer fluorescence with a η_{PL} of 76.8%, which is over nine times higher than the η_{PL} = 8.1% of the B-phase crystals.

Crystal structure

Single crystals with a clear molecular structure and molecular packing can be used to definitely disclose the structure–property relationship between molecular packing and photophysical properties. For **mTPA-9-AN**, two kinds of crystals with completely different stacking modes were determined by a single-crystal XRD experiment (crystallographic data of the two crystals are shown in Table S3, ESI†). The stripe-like B-phase provides edge-to-face stacking of two anthracene moieties, and C–H···π interactions (C–H···π distance: $d1$ = 2.817 Å) play a key role in this arrangement (Fig. 3a and Fig. S8a, ESI†). In addition, there are also C–H···π interactions between the adjacent TPA moieties with $d_{C\text{–}H\cdots\pi}$ of $d3$ = 2.783 Å, $d4$ = 2.834 Å and $d5$ = 2.853 Å, respectively (Fig. S8, ESI†). Such weak intermolecular interactions give rise to the approximate monomer emission (λ_{max} = 455 nm) in the B-phase crystals, similar to the emission (λ_{max} = 469 nm) in THF solution. By contrast, the massive G-phase crystals adopt face-to-face dimeric stacking between two anthracene moieties with a π–π interplanar separation between anthracene moieties of $d2$ = 3.557 Å (Fig. 3b). Essentially, such a large overlap of approximately 40.3% in face-to-face dimeric stacking of anthracence indicates a very strong π–π interaction between anthracence moieties, which may be directly responsible for the so largely red-shifted excimer fluorescence in the G-phase crystals relative to that in the B-phase.[32,33] The intermolecular C–H···π interactions among the TPA unit and its neighboring one in the G-phase crystals were also found and their C–H···π distances are $d6$ = 2.819 Å, $d7$ = 2.845 Å and $d8$ = 2.900 Å, respectively (Fig. S9, ESI†). Additionally, there is C–H···N hydrogen bonding interaction with the C–H···N distance of $d9$ = 2.814 Å (Fig. S9, ESI†) in the G-phase crystals, which does not exist in the B-phase. As we expected, the *meta*-linkage modification between TPA and AN really facilitates the formation of the discrete dimeric stacking of anthracence units as we desired in the G-phase crystals.

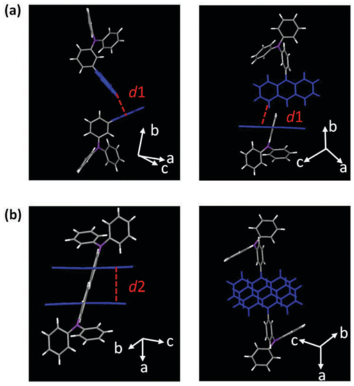

Fig. 3 Stacked pair structure: (a) B-phase crystals ($d1$: 2.817 Å). (b) G-phase crystals ($d2$: 3.557 Å) from the side (left) and top (right) view, respectively. The ratio of the area of overlapped moieties of anthracene rings was estimated from the top view by calculation as the overlapped area divided by the whole area of the anthracene rings.

At the same time, quantum chemical calculations were used to describe the excited state properties of the monomers and dimers from different crystal phases (Fig. S16–S21, ESI†). The natural transition orbital (NTO) of the S_1 state of the B-phase dimer is found to be in good agreement with that of the monomers in terms of both hole-particle distribution and energy (3.6 eV) (Fig. 4a), indicating nearly single molecule excited state properties. In contrast, both holes and particles are equally delocalized over two π–π stacking anthracene moieties for the S_1 state in the G-phase dimer, as well as the obviously stabilized energy (3.4 eV) of the S_1 state, which indicates that a strong state interaction occurs between two monomers. To further examine the nature of the S_1 state, the wave function of the electron–hole pair was calculated by time-dependent density functional theory (TD-DFT), and was plotted in a two-dimensional (2D) color-filled map using Multiwfn software (Fig. 4b). Both the horizontal axis x_i and the vertical axis y_i run over all the non-hydrogen atoms labeled in Fig. S21 (ESI†). Each coordinate point (x_i, y_i) is related to the probability $|\psi(x_i, y_i)|^2$ of finding the electron and hole in the π atomic orbitals of two non-hydrogen atoms x_i and y_i, respectively. The brightness of each coordinate point (x_i, y_i) is directly proportional to the probability of $|\psi(x_i, y_i)|^2$. In Fig. 4b (left), the brightest zones are found in the upper right corner, which represents the LE character localized on one of the anthracene units in the B-phase dimer. As a comparison, the brightest zone is concentrated along the diagonal, indicating the respective LE character of two anthracenes in the G-phase dimer. Simultaneously, the off-diagonal

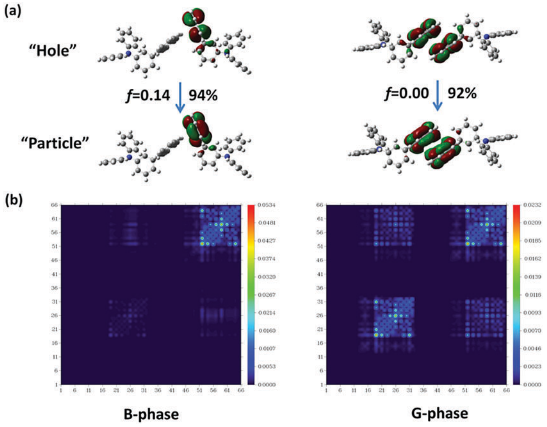

Fig. 4 (a) NTOs from S_0 to S_1 of B-phase (3.6051 eV) (left) and G-phase (3.4270 eV) (right) dimers. (b) Transition density matrix (TDM) color-filled maps of the S_1 state of B-phase and G-phase dimers.

also shows obviously increased brightness, which denotes the incorporation of the CT component from one anthracene to the other in the G-phase dimer (two anthracenes are coherent with each other). Accordingly, the 2D-grid map reveals the excimer state (excited dimer) character in the S_1 state of the G-phase, which actually differs from the excited monomer state in the B-phase. Besides, compared with the ground state geometry in the G-phase dimer, the π–π stacking distance between anthracenes of the S_1 excited state is obviously decreased by 0.351 Å (Fig. S20, ESI†), which means a very unique "compressed" excited state, in favor of the more discrete dimeric stacking in G-phase crystals.

Excimer-induced enhanced emission (EIEE)

In order to better understand high-efficiency excimer fluorescence, we define its mechanism as excimer-induced enhanced emission (EIEE), which is an alternative method to achieve high-efficiency solid-state fluorescence. As for the mechanism of EIEE, the structural factors can be intrinsically responsible for the high-efficiency excimer fluorescence in G-phase crystals. Firstly, compared with the monomer, the excimer-state geometry may possess more rigid chromophores due to the unique "compressed" excited state with the closer and stronger π–π interaction between two anthracene monomers. Thus, the restricted vibrational/rotational motions contribute to the significantly enhanced excimer emission, arising from the effective inhibition of the non-radiative process. What is more, it is worth mentioning that a very highly efficient near-infrared excimer emission has been reported in the Pt(II) complex solid film.[34] As for high efficiency, it can be ascribed to the shallow and repulsive-like potential energy surface (PES) of the dimer in the ground state, which greatly decreases the vibrational overlap between the ground state (dimer) and the excited state (excimer), significantly suppressing vibrational quenching imposed by the energy gap law. Secondly, G-phase crystals present a unique stacking with spatially isolated dimeric anthracenes surrounded by TPA moieties, *i.e.*, there is negligible interaction and communication between dimeric stacks, especially for the "compressed" excimer state. These results are in good agreement with a mono-exponential fluorescence decay of G-phase crystals, indicating a single and pure emissive state from the anthracene excimer. That is to say, the discrete dimeric stacking of anthracene emits high-efficiency fluorescence, which can effectively prevent the formation of energy-trapping "dark" excimer states from larger-size molecular stack to quench dimeric stack fluorescence through non-radiative energy transfer. So the unicity of emissive species plays a crucial role in high-efficiency solid-state photoluminescence, especially for planar polycyclic aromatic molecules which tend to π–π stack in solids. Thirdly, the photodimerization of anthracene as a non-radiative pathway is well inhibited in antiparallel pairwise stacking of anthracene with one-side substitution (**mTPA-9-AN**) (Fig. S15, ESI†), due to the fact that both the nearly "static" excimer and large steric hindrance of TPA prevent the dimers from getting closer to each other. Unlike usual photodimerization of anthracene quenching excimer fluorescence, the disabled photodimerization of anthracene minimizes the non-radiative energy dissipation, which contributes to the enhanced emission. In addition, it is definitely unique for the excimer excited state to possess a compressed geometry with a reduced π–π distance relative to the dimer in the ground state. This point greatly improves the stability and localization of the excimer excited state, avoiding all possible quenching interactions from close contact with the surrounding environment. As a matter of fact, the radiative decay rate (k_r) and non-radiative decay rate (k_{nr}) were estimated on the basis of the known η_{PL} and lifetime (Fig. S10, ESI†). Interestingly, compared with the doped film, the k_r values are dramatically decreased by nearly tenfold in both B-phase and G-phase crystals. For the k_{nr}, there is a certain degree of decrease in the B-phase relative to that of the doped film, but it is sharply decreased in the G-phase by 62-fold in contrast with the doped film and by 44-fold with respect to B-phase crystals. As a result, most of the possible non-radiative deactivations (*e.g.* vibrational quenching, energy transfer and photodimerization) are restricted very well, which is mainly responsible for the EIEE mechanism in G-phase crystals.

Thermally-activated phase transition

More attractively, the fluorescence of B-phase crystals can be converted from blue to green when heated to a certain temperature (445 K). In order to understand this process, we performed a temperature-dependent experiment using the programmed temperature method in ambient atmosphere. The PL spectra were sequentially collected with the increase of temperature, in which the temperature was stabilized for five minutes at each setting value for the system at equilibrium. As the temperature was increased from 295 K to 395 K, the fluorescence intensity was gradually weakened due to the thermally-activated vibrational strengthening non-radiative process, accompanied by the almost unchanged maximum fluorescence wavelength (Fig. 5a). Subsequently, the fluorescence intensity was gradually enhanced along with a still unchanged fluorescence maximum when the temperature was continuously increased to 415 K. Intriguingly, once the temperature reached 425 K, the fluorescence intensity was sharply increased together with an obvious bathochromic shift from blue (455 nm) to green (505 nm), and the whole process was recorded using photographs at different temperatures (in the

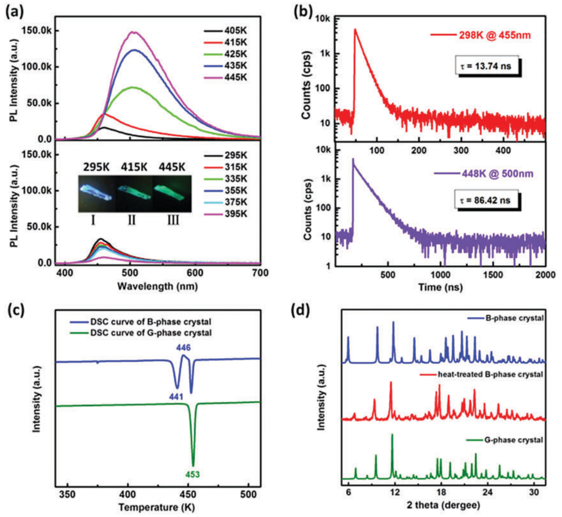

Fig. 5 (a) PL spectra of B-phase crystals with increasing temperature. Inset shows the images of B-phase crystals under UV light (365 nm): (I) at 295 K, (II) at 415 K, (III) at 445 K. (b) Transient PL spectra of B-phase crystals at 298 K monitored at 455 nm and at 448 K monitored at 500 nm. (c) DSC curves of B-phase and G-phase crystals. (d) Powder XRD patterns. XRD patterns represent simulated B-phase crystals, heat-treated B-phase crystals, and simulated G-phase crystals from top to bottom.

inset of I, II and III). This fluorescence behaviour seems to tend towards the greatly enhanced excimer fluorescence in G-phase crystals. At a temperature of 445 K, the fluorescence intensity continued to rise to the maximum, and then it collapsed at the temperature of 455 K due to the melting of the crystals. Preliminarily, such a dramatic change of both fluorescence spectra and intensity should result from the phase transition from the B-phase to the G-phase, involving the transformation of molecular packing in the crystals.[35,36] In addition, the reversible conversion cannot be observed when the temperature was decreased from 445 K to 295 K, which indicates that the heat-treated B-phase is more thermodynamically stable than the B-phase.

To investigate the heat-treated B-phase, the fluorescence decay spectra were further acquired to understand this temperature-dependent fluorescence. Initially, the fluorescence showed a mono-exponential lifetime τ = 13.7 ns at 298 K (Fig. 5b). The fluorescence lifetime was ever-reduced with an increasing temperature ranging from 298 K to 408 K (Fig. S11 and Table S4, ESI†). However, once the temperature reached at 418 K, the lifetime at the wavelength of 450 nm exhibited two components with the addition of a new long lifetime: τ_1 = 7.47 ns (77.58%) and τ_2 = 88.13 ns (22.42%). The two components showed the reverse proportions corresponding to τ_1 = 8.32 ns (29.97%) and τ_2 = 89.32 ns (70.03%), when the wavelength was monitored at 481 nm. This result implies a starting point for the occurrence of phase transition at 418 K, and the increased proportion of the long-lived component indicates the formation of a new emissive species (excited state). And then this long-lived component dominated at higher temperature. At 445 K, the fluorescence lifetime became τ = 86.4 ns (Fig. 5b). As a result, the elongated fluorescence lifetime also indicates that a phase transition occurs from the B-phase to the G-phase when the B-phase crystals are heat-treated.

What is more, the efficiency and lifetime were further determined for heat-treated B-phase crystals at 445 K, when they were cooled down to room temperature. The PL efficiency of η_{PL} = 76.7% in the heat-treated B-phase is almost exactly the same as that of the original G-phase (η_{PL} = 76.8%), along with a practically identical fluorescence lifetime (τ = 155.6 ns *vs.* original τ = 156.2 ns, Fig. S12, ESI†). In terms of the above fluorescence behaviors (spectrum, lifetime and efficiency), it was convincing that G-phase crystals can be achieved from B-phase crystals through a thermally-activated phase transition.

More conclusively, differential scanning calorimetry (DSC) analysis was performed for these two kinds of crystals as shown in Fig. 5c. Both B-phase and G-phase crystals exhibited an identical melting point at 453 K, but an extra endothermal peak at 441 K could be clearly observed for the B-phase crystals. Obviously, the B-phase crystals underwent a phase transition into a stable G-phase. Furthermore, the powder XRD (Fig. 5d) analysis showed the XRD pattern of heat-treated B-phase crystals (above 438 K for 10 minutes). It was strikingly different from that of the pristine B-phase crystals but was almost identical to that of pristine G-phase crystals, which further confirmed that a real thermally-activated crystalline phase transition occurred from the B-phase to the G-phase. In addition, the G-phase crystals originating from heat-treated B-phase and melted B-phase and G-phase crystals were examined by ^{1}H NMR (Fig. S13 and S14, ESI†), suggesting that there was no chemical reaction occurring during the heating process for **mTPA-9-AN**. Additionally, we also found that if we added the B-phase crystals back into the crystal growing mother solution, about one week later, all the B-phase crystals converted into G-phase crystals. In more detail, the calculation results demonstrated that the energy of the G-phase dimer was about 0.225 eV lower than that of the B-phase dimer (Fig. S19, ESI†), and further the enthalpy of the phase transition from B-phase to G-phase crystals could be estimated to be about 12.88 kJ mol^{-1} according to the DSC curve. In terms of structural nature, this also confirmed that G-phase crystals can be achieved from B-phase crystals through a thermally-activated phase transition, together with a completely synchronized change in fluorescence properties. As a whole, on the one hand, it is really the excimer that induces high-efficiency solid-state fluorescence from the discrete dimeric stacking of anthracenes in G-phase crystals in comparison with B-phase crystals. On the other hand, this special crystal stacking of the G-phase can be realized not only from the elaborate molecular design of an anthracene derivative with one-side meta-substituted TPA, but also from the thermally-activated phase transition of the B-phase.

As a prototype application, the enhanced excimer fluorescence from thermally-stimulated phase transition makes a promising smart material for dual-responsive security protection with color-mode. Here, we presented a protoype application in antifake security. In Fig. 6, the ‘‘smiling face’’ pattern was filled with 4-[2-(4′-diphenylaminobiphenyl-4-yl)-phenanthro[9,10-*d*]imidazol-1-yl]-benzonitrile, while the eyes and mouth were replaced by

Fig. 6 Photographs of the "smiling face" pattern before and after heat treatment, demonstrating the potential application in the anti-fake field.

blue powder (obtained by grinding B-phase crystals) of **mTPA-9-AN**.[37,38] Under UV irradiation of 365 nm, the whole face showed the same blue fluorescence. Once heated to 445 K, the color of the eyes and mouth changed to brightly green excimer fluorescence. Furthermore, this simple pattern with security information will inspire us to develop more special and more practical applications in the future.

Conclusions

In conclusion, a *meta*-triphenylamine substituted anthracene derivative was synthesized, and its two crystalline phases (B-phase and G-phase) were obtained by slow evaporation in compositional solvents. The large difference of molecular packing in the crystals gave rise to phase-dependent photophysical properties. Compared with the B-phase, G-phase crystals exhibited nearly tenfold fluorescence efficiency from excimer species (η_{PL} = 76.8%) with much longer lifetime (τ = 156.2 ns), which is attributed to excimer-induced enhanced emission (EIEE). The essence of EIEE in the G-phase can be ascribed to the following several aspects: the "compressed" excimer state to significantly suppress vibrational quenching of non-radiative decay; the discrete dimeric stacking of anthracene to avoid the formation of the energy-trapping large-size excimer "dark" state for the effective inhibition of non-radiative energy transfer; the large steric hindrance of *meta*-TPA to disable photodimerization of anthracene for the excludable photochemical quenching of non-radiative energy dissipation. Besides, this kind of discrete dimeric stacking in the G-phase can be achieved not only from rational molecular design, but also from thermally-activated phase transition of the B-phase. Evidently, it is really excimer formation that contributes to high-efficiency solid-state fluorescence, corresponding to the discrete dimeric stacking of anthracenes in G-phase crystals. Once again, this result validates a new strategy for building discrete dimeric stacking of planar polycyclic aromatic molecules in the solid state to realize high-efficiency fluorescence by the excimer-induced enhanced emission (EIEE) mechanism.

Conflicts of interest

There are no conflicts to declare.

Acknowledgements

This work was supported by the National Basic Research Program of China (2015CB655003), the National Natural Science Foundation of China (51673083 and 51473063), and the Open Project Foundation of the State Key Laboratory of Luminescence and Applications (Changchun Institute of Optics, Fine Mechanics and Physics of the Chinese Academy of Science, SKLA-2016-04).

Notes and references

1 S. Lamansky, P. Djurovich, D. Murphy, F. Abdel-Razzaq, H. E. Lee, C. Adachi, P. E. Burrows, S. R. Forrest and M. E. Thompson, *J. Am. Chem. Soc.*, 2001, **123**, 4304–4312.
2 T. W. Lee, J. Zaumseil, S. H. Kim and J. W. P. Hsu, *Adv. Mater.*, 2004, **16**, 2040–2045.
3 J. Zaumseil and H. Sirringhaus, *Chem. Rev.*, 2007, **107**, 1296–1323.
4 C. Wang, H. Dong, W. Hu, Y. Liu and D. Zhu, *Chem. Rev.*, 2012, **112**, 2208–2267.
5 I. D. W. Samuel and G. A. Turnbull, *Chem. Rev.*, 2007, **107**, 1272–1295.
6 H. Osaki, C. M. Chou, M. Taki, K. Welke, D. Yokogawa, S. Irle, Y. Sato, T. Higashiyama, S. Saito, A. Fukazawa and S. Yamaguchi, *Angew. Chem., Int. Ed.*, 2016, **55**, 7131–7135.
7 S. Ghosh, A. Ganguly, M. R. Uddin, S. Mandal, M. A. Alam and N. Guchhait, *Dalton Trans.*, 2016, **45**, 11042–11051.
8 G. Zhang, G. Yang, S. Wang, Q. Chen and J. S. Ma, *Chemistry*, 2007, **13**, 3630–3635.
9 J. Mei, Y. Hong, J. W. Y. Lam, A. Qin, Y. Tang and B. Z. Tang, *Adv. Mater.*, 2014, **26**, 5429–5479.
10 J. Mei, N. L. Leung, R. T. Kwok, J. W. Lam and B. Z. Tang, *Chem. Rev.*, 2015, **115**, 11718–11940.
11 Y. Hong, J. W. Y. Lam and B. Z. Tang, *Chem. Soc. Rev.*, 2011, **40**, 5361–5388.
12 R. H. Friend, R. W. Gymer, A. B. Holmes, J. H. Burroughes, R. N. Marks, C. Taliani, D. D. C. Bradley, D. A. Dos Santos, J. L. Bredas, M. Logdlund and W. R. Salaneck, *Nature*, 1999, **397**, 121–128.
13 S. A. Jenekhe and J. A. Osaheni, *Science*, 1994, **265**, 765–768.
14 P. N. Taylor, M. J. O'Connell, L. A. McNeill, M. J. Hall, R. T. Aplin and H. L. Anderson, *Angew. Chem., Int. Ed.*, 2000, **39**, 3456–3460.
15 L. H. Chen, S. Xu, D. McBranch and D. Whitten, *J. Am. Chem. Soc.*, 2000, **122**, 9302–9303.
16 V. I. Adamovich, S. R. Cordero, P. I. Djurovich, A. Tamayo, M. E. Thompson, B. W. D'Andrade and S. R. Forrest, *Org. Electron.*, 2003, **4**, 77–87.
17 B. Stender, S. F. Voelker, C. Lambert and J. Pflaum, *Adv. Mater.*, 2013, **25**, 2943–2947.
18 G. Li, D. Zhu, T. Peng, Y. Liu, Y. Wang and M. R. Bryce, *Adv. Funct. Mater.*, 2014, **24**, 7420–7426.
19 L. S. Kaanumalle, C. L. D. Gibb, B. C. Gibb and V. Ramamurthy, *J. Am. Chem. Soc.*, 2005, **127**, 3674–3675.
20 H. Liu, L. Yao, B. Li, X. Chen, Y. Gao, S. Zhang, W. Li, P. Lu, B. Yang and Y. Ma, *Chem. Commun.*, 2016, **52**, 7356–7359.
21 S. Sekiguchi, K. Kondo, Y. Sei, M. Akita and M. Yoshizawa, *Angew. Chem., Int. Ed.*, 2016, **55**, 6906–6910.
22 G. Han, D. Kim, Y. Park, J. Bouffard and Y. Kim, *Angew. Chem., Int. Ed.*, 2015, **54**, 3912–3916.

23 J.-Y. Hu, Y.-J. Pu, Y. Yamashita, F. Satoh, S. Kawata, H. Katagiri, H. Sasabe and J. Kido, *J. Mater. Chem. C*, 2013, **1**, 3871–3878.

24 S. P. Jagtap, S. Mukhopadhyay, V. Coropceanu, G. L. Brizius, J. L. Bredas and D. M. Collard, *J. Am. Chem. Soc.*, 2012, **134**, 7176–7185.

25 D. Kim and J. L. Bredas, *J. Am. Chem. Soc.*, 2009, **131**, 11371–11380.

26 H. Liu, D. Cong, B. Li, L. Ye, Y. Ge, X. Tang, Y. Shen, Y. Wen, J. Wang, C. Zhou and B. Yang, *Cryst. Growth Des.*, 2017, **17**, 2945–2949.

27 W. Li, Y. Pan, L. Yao, H. Liu, S. Zhang, C. Wang, F. Shen, P. Lu, B. Yang and Y. Ma, *Adv. Opt. Mater.*, 2014, **2**, 892–901.

28 A. R. Mallia, R. Ramakrishnan, M. A. Niyas and M. Hariharan, *CrystEngComm*, 2017, **19**, 817–825.

29 L. O. Palsson and A. P. Monkman, *Adv. Mater.*, 2002, **14**, 757–758.

30 P. E. Fielding and R. C. Jarnagin, *J. Chem. Phys.*, 1967, **47**, 247–252.

31 M. Jaseer and E. Prasad, *J. Photochem. Photobiol., A*, 2010, **214**, 248–256.

32 Z. Zhang, Y. Zhang, D. Yao, H. Bi, I. Javed, Y. Fan, H. Zhang and Y. Wang, *Cryst. Growth Des.*, 2009, **9**, 5069–5076.

33 T. Hinoue, Y. Shigenoi, M. Sugino, Y. Mizobe, I. Hisaki, M. Miyata and N. Tohnai, *Chem. – Eur. J.*, 2012, **18**, 4634–4643.

34 K. Tuong Ly, R. W. Chen-Cheng, H. W. Lin, Y. J. Shiau, S. H. Liu, P. T. Chou, C. S. Tsao, Y. C. Huang and Y. Chi, *Nat. Photonics*, 2016, **11**, 63–68.

35 S. Hisamatsu, H. Masu, M. Takahashi, K. Kishikawa and S. Kohmoto, *Cryst. Growth Des.*, 2015, **15**, 2291–2302.

36 M.-S. Yuan, D.-E. Wang, P. Xue, W. Wang, J.-C. Wang, Q. Tu, Z. Liu, Y. Liu, Y. Zhang and J. Wang, *Chem. Mater.*, 2014, **26**, 2467–2477.

37 S. Zhang, L. Yao, Q. Peng, W. Li, Y. Pan, R. Xiao, Y. Gao, C. Gu, Z. Wang, P. Lu, F. Li, S. Su, B. Yang and Y. Ma, *Adv. Funct. Mater.*, 2015, **25**, 1755–1762.

38 S. Zhang, Y. Dai, S. Luo, Y. Gao, N. Gao, K. Wang, B. Zou, B. Yang and Y. Ma, *Adv. Funct. Mater.*, 2017, **27**, 1602276.